PREPARATION AND PHOTOCATALYTIC PROPERTIES OF Ag/Graphene/TiO_2 COMPOSITES

S. Y. LI[a], J. H. FENG[a*1], H. W. CHEN[a], J. Y. LU[a], D. M. YAO[a], H. Y. ZHANG[a], Y. L. QIN[b]

[a]*College of Chemical and Biological Engineering, Hechi University, Yizhou 546300, China*

[b]*Application and research center of agricultural biotechnology, Hechi University, Yizhou546300, China*

The composite catalysts were prepared by two-step photothermal synthesis, and the morphology, structure and catalytic performance of the Ag/graphene/TiO_2 composite were characterized by SEM, FT-IR, XRD, etc. The results showed that the composites were prepared successfully by Ag depositing on TiO_2 compounded with graphene, and solid UV diffuse reflection test showed that Ag/Graphene/TiO_2 composites had the greatest enhancement in the absorption of visible light. The results showed that among four kinds materials, the methyl orange's degradation rate of Ag/Graphene/TiO_2 in simulated visible light reached best, whose degradion was 4.25 times that of pure TiO_2. The number of photocatalytic experiments showed that Ag/Graphene/TiO_2 photogenerated electrons and the corresponding generated O_2· dominated the catalysis.

(Received October 13, 2020; Accepted February 15, 2021)

Keywords: TiO_2, Silver, Graphene, Photocatalysis

1. Introduction

TiO_2 has the advantages such as oxidizing ability, high chemical stability, nontoxicity, and so on [1-4]. So it has become the most commonly used photocatalytic material [5-7]. However, pure TiO_2 photocatalyst has some shortcomings such as low efficiency of solar light utilization, and easy recombination of photogenerated carriers [8-11], so TiO_2 needs to be modified to improve its visible photocatalytic activity. Aiming at the problems existing on TiO_2, we can modify the TiO_2 surface with doping metal and non-metal to expand the range of light response and improve its photocatalytic efficiency[12-14]. Basing on nonmetallic doping of carbon-based components such as graphene, carbon nanotubes, it really helps to improve the photocatalytic performance of TiO_2 materials. As a novel nanomaterial, graphene has attracted much attention due to its high surface adsorption, large specific surface area and excellent charge transfer performance, and excellent photocatalytic activity for a certain amount of dye pollutants [15-18]. Lin and his co-workers [19] reported that TiO_2-graphene nanocomposites exhibited significantly higher photocatalytic activity for pharmaceuticals, which was strongly affected by the amount of

* Corresponding authors: chuntian1619@163.com

graphene in the hybrids. Therefore, graphene is also widely used in composites to improve the photocatalytic performance of target products [20, 21]. As reported in many literatures, the doping of precious metals such as Pt[22,23], Ag[24,25], Au[26, 27] can provide photocatalytic activity. Ag , as one of the lower cost noble metals and relatively small modification toxicity, the proper addition of its amount can change the surface properties of TiO_2 by increasing the separation and extending wavelength response of photogenerated electron-hole pairs [24][28-31]. Under UV irradiation, the photocatalytic efficiency of composites which was adding 0.5% Ag nanospheres on p25 was about 1.5 times that of pure p25[32]. Shirley P.Onkani and his co-workers found that the Ag doping semiconductor obtained from TiO_2, ZnO and ZnS all enhanced photocatalysts, the Ag-doped TiO_2 was more effective than the ZnO and ZnS species[33]. These reports suggested that Ag addition on supported substrate photocatalytic materials can help improve their photocatalytic performance.

In this work, Ag/Graphene/TiO_2 composites were synthetised using tetrabutyl titanate as titanium source to make nano-sized TiO_2 by hydrothermal method firstly, silver deposited by uv-light irradiation using silver nitrate as material secondly, and graphene directly loading to TiO_2 with silver nitrate at the same time. Then it was explored the degradation effect and the degradation mechanism of composite materials on methyl orange (MO). The paper was purposed to improve the utilization rate of TiO_2 composites to enhance their photocatalytic properties on organics.

2. Experimental

2.1. Laboratory reagents

Tetrabutyl titanate(TBOT), silver nitrate($AgNO_3$), Tween-80, anhydrous ethanol, methyl orange, p-benzoquinone, sodium oxalate, disodium ethylenediamine tetraacetate (EDTA), isopropanol, All materials were analytically pure and used without further purification. The deionized water(DI) was used during the experimental process. Graphene purchased from TCI Development Co., Ltd.

2.2. Synthesis of Ag/Graphene/TiO_2

A certain amount of anhydrous ethanol was mixed with 2 mL of tween-80 and magnetically stir for 10 min at room temperature, and then 1 mL of tetrabutyl titanate was added drop by drop with continuing to magnetically stir 10 min. After then, solution was transferred to Teflon-lined autoclave, and heated at 160 ℃ for 8h. After the reaction solution was cooled, a certain amount of graphene and silver nitrate solution was added and scattered by ultrasonic dispersion for 15 min. At last, final solution was irradiated by ultraviolet light for a certain time. The resulting samples were washed with deionized water and ethanol several times, and then dried in a vacuum oven under 80 ℃.

The pure TiO_2 was obtained by without adding graphene and silver nitrate to solution which mentioned above whose were made of Ag/Graphen/TiO_2. The same as graphene/TiO_2 and Ag/TiO_2 as without adding silver nitrate and graphene.

2.3. Characterization of catalyst

Field Emission Environment Scanning Electron Microscope (FEI Quanta 200FEG, Dutch Philips) was used to test the morphologies of prepared samples. X-ray powder diffraction pattern(XRD) was obtained by a D/ Max 3B X-ray diffractometer (Japan) with Cu Kα irradiation source (λ=1.5418 Å) through the 2θ range from 5° to 90. Fourier-transform infrared(FT-IR) spectra with KBr powder-pressed pellets were characterized by Nicolet 6700(USA). The weight loss of different materials was measured by differential calorimeter, the temperature range was 25 ℃ -900 ℃, and the heating rate was 10 ℃ / min(Future Ltd.,China). X-ray photoelectron spectroscopy (XPS) spectra of the samples were acquired using a Gammadata-scienta ESCA 200 hemispherical analyzer equipped with an Al X-ray source (1486.6 eV). All binding energy values were corrected by calibrating the C 1 s peak at 284.6 eV. Bruker Dispersive Raman Spectrometer (model: Senterra) with 785 nm laser excitation was used to record the Raman spectrum of the samples.The optical properties of the samples were characterized by a UV-2600 ultraviolet/visible diffuse reflectance spectrophotometer (DRS), during which BaSO4 was employed as the internal reflectance standard. The concentration of Methyl Orange dyes was obtained by Uv-Vis Spectrophotometer (model: 8453, agilent, USA).

2.4. Evaluation of photocatalytic performance

The adsorbent ability and photodegradable activity of prepared samples were evaluated by remove of MO. In a typical process, 0.1g catalyst in 20 mL 30 mg/L MO solution were placed in a quartz vessel, the suspension was stirred at dark for 30 minutes to evaluated the adsorbent ability. After then , simulated ultraviolet light (Xenon light source using bandpass 380 nm filter) or the simulated visible light (Xenon light source using cut-off 400 nm filter) was turned on for 120 minutes . A certain amount of solution was taken out every 20 min and filterd with 0.22 um microporous filter membrane to remove the catalysts. The photodegradable activity was observed by measuring the absorbance of the filtrate by ultraviolet spectrophotometer. The degradation rate (D%) is expressed as follows:

$$D\% = \frac{C_0 - C_t}{C_0} \times 100\% \quad (1)$$

where C_0 and C_t respectively denoted the initial concentration and the concentration at a certain moment.

2.5. Mechanism of photocatalysis

Photodegradation mechanism of Ag/graphene/TiO_2 composite photocatalyst was studied by adding the same equal volume solution of distilled water (blank experiment), isopropanol (hydroxyl radical trapping agent), p-benzoquinone (superoxide radical trapping agent), sodium oxalate solution (hole trapping agent), EDTA (photoelectronic trapping agent) respectively on the base of the typical photocatalytic performance under visible light . The absorbance of MO solution at different time was recorded and the degradation mechamism was study by the effect of each quencher on the degradation rate.

3. Results and discussion

3.1. Characterization of composites

3.1.1. SEM analysis of composites

The morphologies of prepared samples were characterized by SEM. As shown in Fig. 1a, The TiO_2 micrographs showed that the spherical particles accumulated into hollow shape. Fig. 1b distributed on the surface of Ag/TiO_2, it demonstrated that Ag does not change the morphology of TiO_2, and it scattered on the spherical particles which was seen by loading as bright spots. Fig.1c and Fig.1d which represented $Graphene/TiO_2$ and $Ag/Graphene/TiO_2$ showed that thin-sheet graphene sheets can be seen, but the addition of graphene significantly changes the morphology of the $Graphene/TiO_2$ and $Ag/Graphene/TiO_2$ materials from the spherical stacked hollow shape to a bulk morphology.

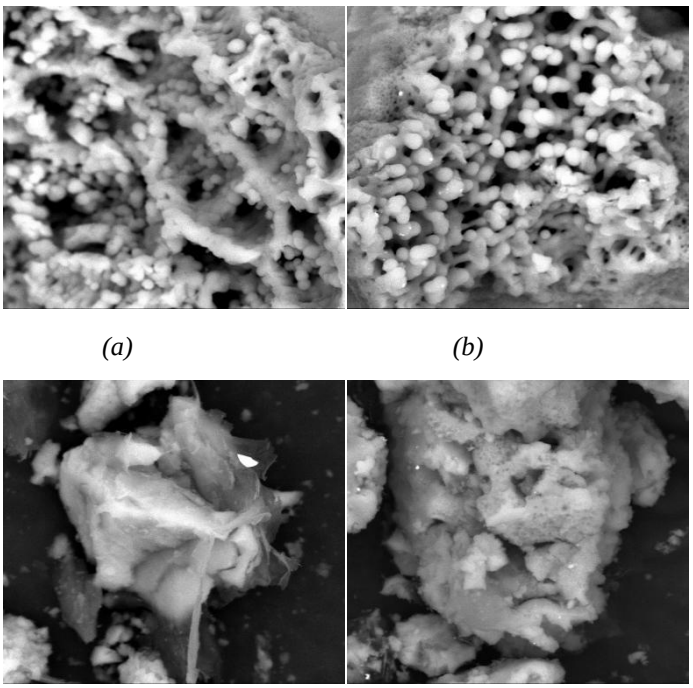

(a) *(b)*

(c) *(d)*

Fig. 1. SEM diagram of composites (a:TiO_2, b:Ag/TiO_2, c:$Graphene/TiO_2$,d: $Ag/Graphene/TiO_2$).

3.1.2. FT-IR analysis of composites

The Infrared spectra of composites were showed in Fig. 2. The positions of the peaks of the four materials were basically the same, and there was a broad and strong absorption peak in the range of 500 cm^{-1}-800 cm^{-1} , which was assigned to the stretching vibration and variable angle vibration peak of Ti—O—Ti bond of the TiO_2 crystal. The peaks located at 1396 cm^{-1} and 1640 cm-1 corresponding to C-O and C=O stretching vibrations of COOH groups edging the material, respectively [34-36]. The broad diffraction peaks from 3000 cm^{-1} to 3500 cm^{-1} could be attributed to the stretching vibration of O-H bond. The FT-IR peaks of the TiO_2, $Graphene/TiO_2$, Ag/TiO_2, $Ag/Graphene/TiO_2$ showed there was little differences in the position of the peaks, indicating that the addition of Ag and graphene did not affect the crytal of TiO_2. The corresponding characteristic signal peak of Ag and graphene were not detected, may be owing to low quantity or weak intensity of corresponding characteristic peak.

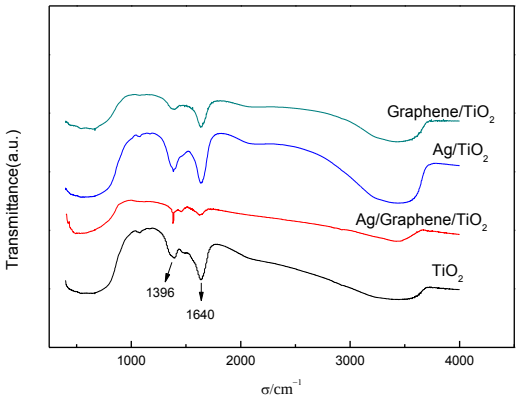

Fig. 2. FT-IR of composites.

3.1.3. XRD analysis of composites

The crystalline phases of materials were examined by XRD patterns(Fig. 3). It showed that the peak position of each material was basically the same. The diffraction peaks of the materials located 2θ=25.28°, 37.80°, 48.05°, 55.06°, 62.86°, 70.31°, 75.03° and 82.65° corresponded to the (101), (004), (200), (211), (204), (220), (215) and (224) crystal planes of the anatase TiO_2 respectively (JCDPS cards 21-1272). The spectrograms of Graphene/TiO_2 and the Ag/Graphene/TiO_2 showed that they both had a weak peak located at 2θ=25.3, mainly duing to the characteristic peak of graphene [37,38]. The diffraction peaks of silver (Ag) were not detected in the XRD diagram, because of excessive dispersion of Ag on the surface of TiO_2 and low content of Ag [39]. As shown, the composition did not change the main crystal form of TiO_2.

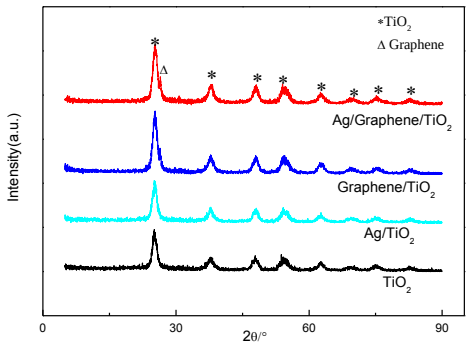

Fig. 3. XRD diagram of composites.

3.1.4. TG analysis of composites

The thermal weight loss of materias were examined by TG patterns(Fig. 4). It showed that all materials had significant weight loss before 100℃, mainly because of the volatilization of the moisture which presented in the material when heated. The loss of water in the structure of the materials resulted obvious mass loss between 250 ℃and 350 ℃. The weight loss of Graphene/TiO_2 and Ag/Graphene/TiO_2 after 400℃ was obvious mainly attributing to the pyrolysis loss of graphene at high temperature. The total weight loss rates of TiO_2, Ag/TiO_2, Graphene/TiO_2, Ag/Graphene/TiO_2 were 8.861 wt %, 10.78 wt %,12.72 wt %,15.76 wt % in wt respectively.

Overall, the addition of composite components had a certain effect on the thermal loss of the material.

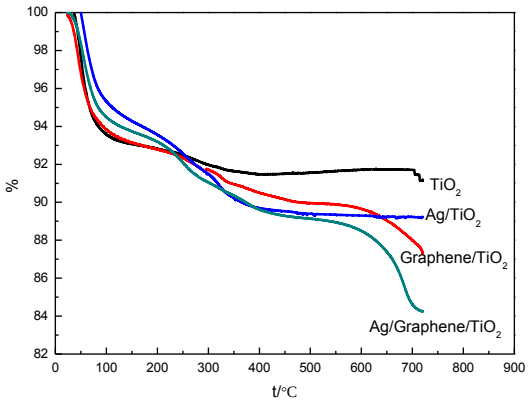

Fig. 4. TG diagram of materials.

3.1.5. Raman spectroscopy analysis of composites

Fig. 5 demonstrates Raman spectra of TiO_2, Ag/TiO_2, $Graphene/TiO_2$, $Ag/Graphene/TiO_2$ microspheres respectively. The figure demonstrates several characterized bands at 146.8, 391.7, 511.2 and 634.4 cm^{-1} , corresponding to Eg_1, B_{1g}, A_{1g}, and Eg_2 modes of anatase phase of TiO_2 respectively[40,41]. Because of the structure of graphitized structures, two typical bands of D and G bands were found at 1351 cm^{-1} and 1651 cm^{-1} on the $Graphene/TiO_2$ and $Ag/Graphene/TiO_2$'s spectra, which was corresponding to disorder carbon and sp^2 hybridized carbon respectively[42]. It was noted that the strength of D and G band peaks on $Ag/Graphene/TiO_2$ was stronger than that of $Graphene/TiO_2$ because of the Raman enhancement effect of Ag.

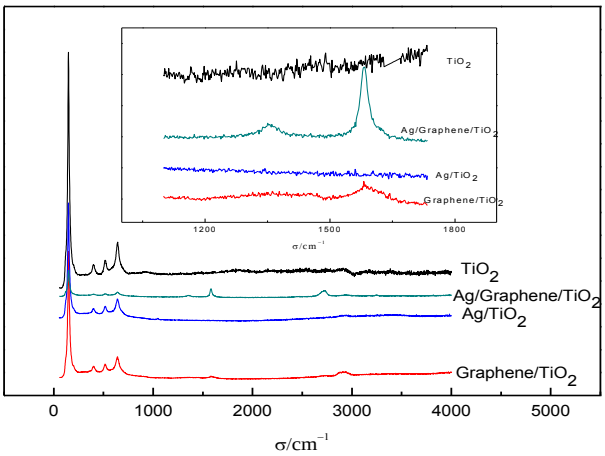

Fig. 5. Raman spectra of materials.

3.1.6. XPS analysis of Ag/Graphene/TiO₂

The surface composition and chemical state of $Ag/Graphene/TiO_2$ was further investigated using X-ray photoelectron spectroscopy. The survey XPS spectra shows the presence of Ti, O, C and Ag elements in the prepared sample without other impurity elements in Fig. 6(a) . The binding energies in the obtained XPS spectra are calibrated using C1s at 284.6 eV. The two characteristic peaks at 459.45eV and 465.12eV are observed in Fig. 6(b), which coincided with the Ti $2p_{3/2}$ orbit

at 459.45 eV, coincided with the orbit of Ti $2p_{1/2}$ at 465.12 eV. Fig. 6(c) demonstrated the XPS spectrum of O 1s.

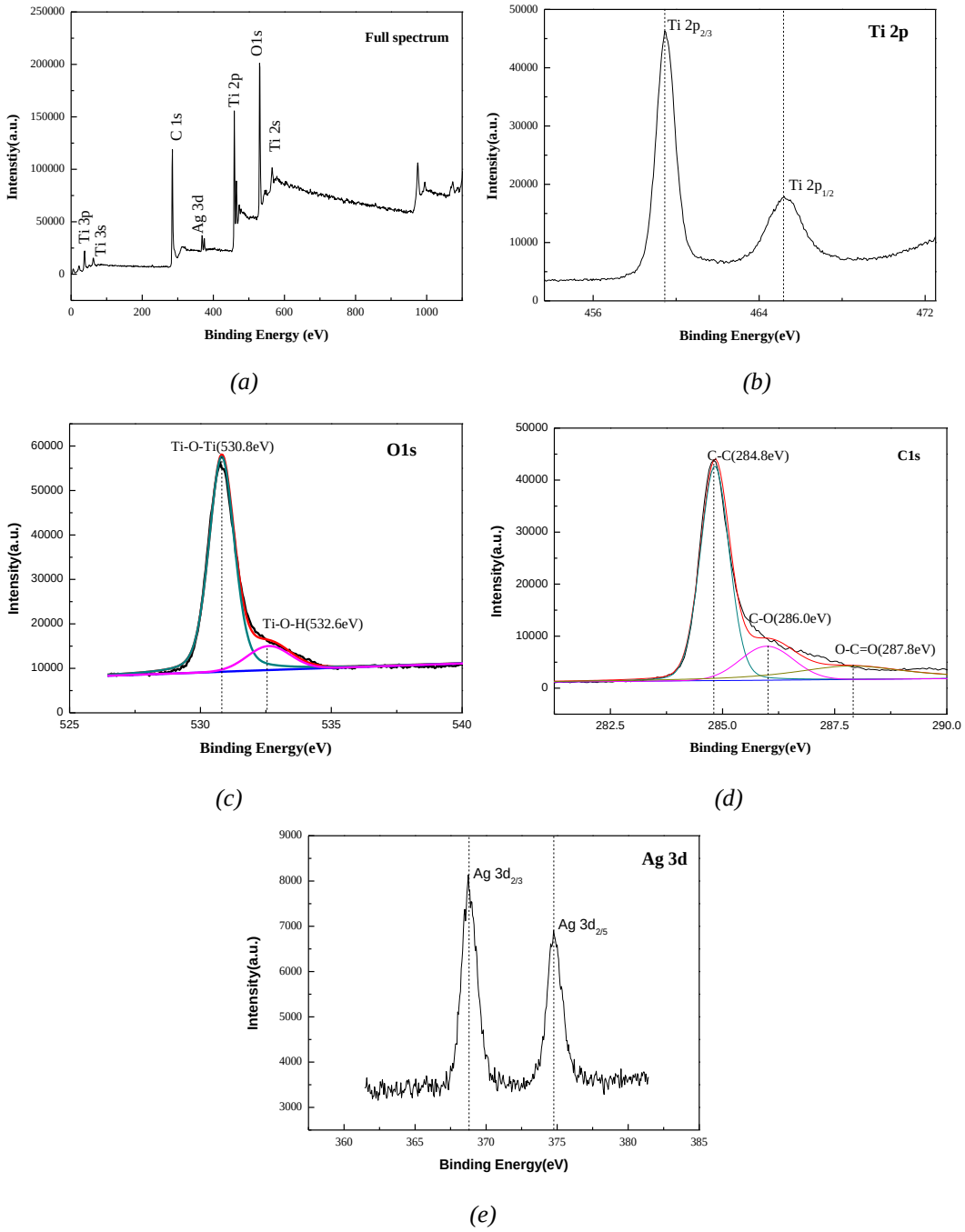

Fig. 6. XPS spectra of Ag/Graphene/TiO_2: (a) survey, (b)Ti 2p , (c) O 1 s, (d) C 1s, (e) Ag 3d.

By using Gaussian-Lorentzian peak fitting, the O 1s spectrum can be deconvolved into two peaks with binding energies of 530.8 eV and 532.6 eV, which correspond to Ti-O-Ti (lattice O) and Ti-O-H. Similarly, C 1s spectrum in Fig. 6(d) can be deconvolved into three peaks at 284.8eV，286.0eV and 287.8 eV. The binding energy at 284.8 eV ascribing to sp^2 hybridized carbon in graphene. On binding energy of 286.0 eV and 287.8 eV ascribing to the C-O and O-C=O bond,

which all belong to oxygen bound species. Two characteristic peaks of 368.73 eV and 374.69eV can be observed in Fig. 6(e) that correspond to Ag $3d_{5/2}$ and Ag $3d_{3/2}$ in metallic Ag [8,43]. The data is proved the existence of TiO_2, Ag and Graphene in the composite components.

3.1.7 Diffuse reflectance spectra analysis of materials

The Diffuse reflectance spectra curve was used to analyze the optical properties of materials. As shown in Fig. 7a, the optical absorption curves for all specimens were nearly identical below the 400 nm wavelength. At wavelengths longer than 400 nm, compared to the bare TiO_2, the materials introduced Ag or graphene have an increasement at the absorption intensity and present a red shift in varying degrees. Especially Ag/Graphene/TiO_2 showed the strongest absorption of light in the visible band, mainly due to the strong localized surface plasmon resonance (LSPR) effect of metal Ag nanoparticles[8][44] and the sensitization effect of carbonaceous materials [8][45].

The optical absorption ability is crucial index for photocatalysis process. The photocatalysis performance could be mainly improved by tuning the band gap energy of TiO_2 into the visible region. Furthermore, the band gaps of mateirals were calculated by Eq.(2):

$$(\alpha h\upsilon)^{n} = A(h\upsilon - E_g) \quad (2)$$

where α, h, υ, E_g and A are the absorption coefficient, Planck's constant, light frequency, band gap and a constant, respectively. The index n relies on the type of electronic transition of semiconductor, where n=2 for direct-gap semiconductor and n=0.5 for indirect-gap semiconductor. For TiO_2 and other materials, n=2. The relevant Kubelka–Munk transition reflectance spectra were shown in Fig. 7b. The band gap can be calculated from the intercept of the tangent to the plot of $(\alpha h\upsilon)^2$ vs. (hv). As shown in Fig. 7b, the band gap of pure TiO_2 was 3.18 eV, which is close to 3.2 eV by previous literatures [45]. The band gap decreased obviously while introducing Ag and graphene. The band gaps of Graphene/TiO_2, Ag/TiO_2, Ag/Graphene/TiO_2 samples were 3.08, 3.01 and 2.64eV, respectively.

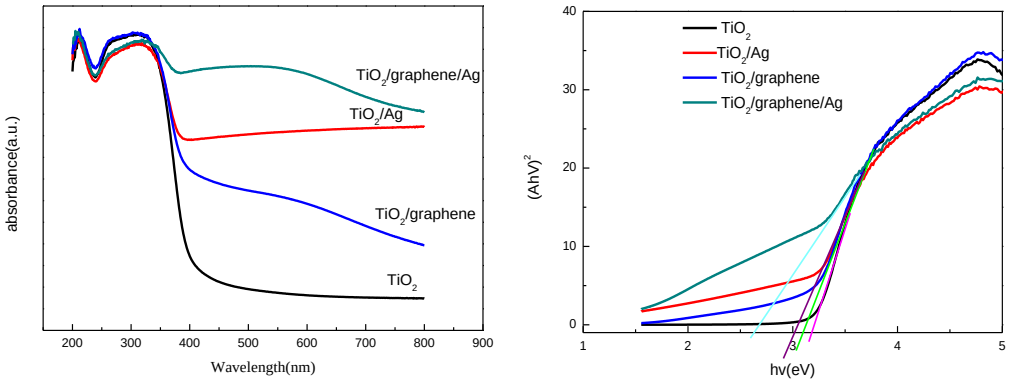

(a) *(b)*

Fig. 7. (a)DRS absorption spectra and (b) plot of $(\alpha h\upsilon)^2$ versus energy (hv) of TiO_2 , Ag/TiO_2, Graphene/TiO_2 and Ag/Graphene/TiO_2 respectively.

3.2. Photocatalytic properties of composites under different light sources

3.2.1. Photocatalytic properties of composites under ultraviolet light

Photocatalytic activity of all the prepared materials was researched by photodegradation of MO dye under UV–Vis light irradiation. As showed in Fig.8a, the photocatalytic results indicated that Ag/Graphene/TiO_2 delivered maximum photocatalytic property when compared to other photocatalyst degrading MO by 82.53% in 150 min. And MO is degraded up to 42.65%, 48.32% and 69.64% for TiO_2, Graphene/TiO_2 and Ag/TiO_2 a in 150 min respectively.

At relatively low concentration of dye, the Langmuir– Hinshelwood model was reduced to the pseudo first order model [8,46]. This model expressed by Eq. (3):

$$-In\frac{C_t}{C_0} = kt$$

where k is the first-order rate constant. This model is generally used for the photocatalytic degradation process if the initial concentration of the pollutant is low. TiO_2 presents an apparent reaction rate constant k of 0.0039min^{-1} under the irradiation of ultraviolet ligh. While, the samples of Graphene/TiO_2, Ag/TiO_2 and Ag/Graphene/TiO_2 showed the reaction rate constant of 0.0049min^{-1}, 0.0166min^{-1} and 0.0211min^{-1} respectively. The equation fits a better linear correlation.

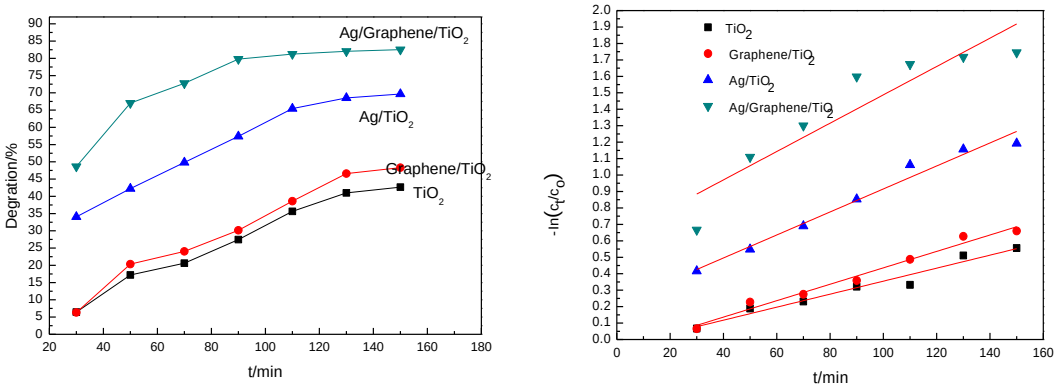

(a) *(b)*

Fig. 8. (a) Photocatalytic degradation of MO (b) the corresponding pseudo-first-order kinetics of the photocatalytic activity degradation of MO by materials under ultraviolet radiation.

3.2.2. Photocatalytic properties of composites under visible light

Fig.9a showed the degradation curve under visible light. As it shows, the degradation rates of TiO_2, Graphene/TiO_2, Ag/TiO_2 and Ag/Graphene/TiO_2 were 23.11%, 28.23%, 92.85% and 98.23% respectively. Obviously, the degradation rate of Ag/Graphene/TiO_2 composites was optimal and it was 4.25 times that of pure TiO_2. The photodegradation performance of TiO_2 and Graphene/TiO_2 under visible light is decreased compared with what under ultraviolet light. Conversely, the degradation rate under visible light of Ag/TiO_2 and Ag/Graphene/TiO_2 materials was higher than that of under ultraviolet light, and the photocatalytic performance of the composite was better under white light. By a pseudo-first-order kinetic fitting, the TiO_2, Graphene/TiO_2, Ag/TiO_2, Ag/Graphene/TiO_2 rate constants were 0.00166 min^{-1}, 0.00211min^{-1}, 0.01891min^{-1} and 0.0271 min^{-1} respectively. Under visible light irradiation, the photocatalytic activity of the bare

TiO_2 was very low because the illumination energy is below the band-gap energy of TiO_2. The boosting of photocatalytic activity was attributed to the red-shift of the wavelength response range due to surface plasmon resonance (SPR) effect of Ag and the minimizing of electron–hole recombination rate for increasing the lifetime of the electron–hole pairs by Ag and graphene[46].

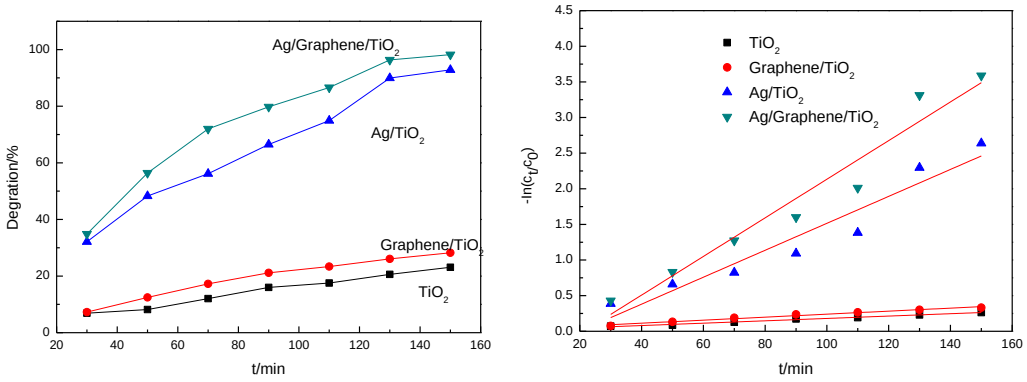

(a) *(b)*

Fig. 9. (a) Photocatalytic degradation of MO (b)the corresponding pseudo-first-order kinetics of the photocatalytic activity degradation of MO by materials under visible radiation.

3.3. Photocatalytic mechanism

In order to study the active groups produced in the photocatalytic process, four trapping agents were added to the experiment to capture the active groups respectively. The experimental results were shown in figure 10. The degradation rate list as: Blank> isopropanol> sodium oxalate>p-benzoquinone >EDTA, it showed that the degradation rate of MO mixed with quencher wer all decreased, the degradation rate mixed with EDTA was lower than that of sodium oxalate, and the degradation rate of solution mixed with p-benzoquinone was lower than that with isopropanol solution, meaning in the photocatalytic process, photogenerated electrons and corresponding generated $O_2\cdot$ dominating the degradation process. A possible mechanism of photocatalytic degrade MO under visible light irradiation was shown in Fig11, under irradiation, the mateirials nanoparticles were excited. Electron transition from valence band (VB) to conduction band (CB), left a hole on VB. The photogenerated electron can be transferred by graphene and accepted by Ag nanoparticles to achieve the separation of e-h^+ pairs. The photogenerated electron reacted with surface O_2 to form superoxide ions ($O_2^{-}\cdot$), which had strong oxidizing properties of degrading MO effectively. The left hole as the minor oxidizer, will react with water to generate hydroxyl radicals (·OH), which could also oxidize dye into nontoxic water and CO_2.

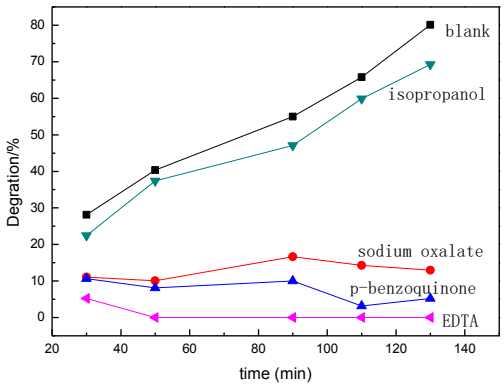

Fig. 10. Effect of radical scavengers on MO's degradation.

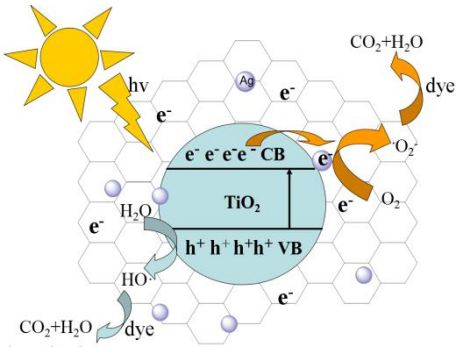

Fig. 11. The scheme mechanism of photocatalytic degradation of MO for Ag/Graphene/TiO_2.

4. Conclusions

In conclusion, the above study proved that the silver-modified TiO_2 microspheres compounded with graphene delivered good photocatalytic activity. The silver nanoparticles and graphene was successfully compounded well with TiO_2 microspheres by two-step photothermal method, and the strong interaction between composite component and TiO_2 microspheres promoted the transfer of electrons. This was confirmed by SEM, XRD, Raman, TG, XPS and UV-Vis absorption spectra. Compare to ultraviolet light, the degradation of Ag/Graphene/TiO_2 in the simulation of white light was up to the best which reached 98.23% at 150 min among the four materials, whose degradation was 4.25 times that of pure TiO_2.

A possible mechanism of photocatalytic degradation of MO due to rapid generation of electrons and photons because of conductive Ag and graphene under visible light irradiation , and the photo-generated electrons and corresponding generated $O_2^{-}\cdot$ dominate the catalysis in the photocatalytic process of materials. The preparation of silver modified TiO_2 composite compounded with graphene by two-step photothermal method provides a good reference for application research of other metal or non-metallic ternary nano-materials composites in the further.

Acknowledgments

The work was supported by the National Natural Science Foundation of China (21563010); Guangxi Provincial Natural Science Foundation of China(2018GXNSFAA138140); Guangxi Basic Enhancement Project for Young People of China (2020KY15019).

References

[1] J. R. Chen, F. X. Qiu, W. Z. Xu, S. S. Cao, H. J. Zhu, Applied Catalysis A General **495**, 131 (2015).
[2] L. L. Yang, Q. Q. Sang, J. Du, M. Yang, X. L. Li, Y. Shen, X. X. Han, X. Jiang, B. Zhao, Physical Chemistry Chemical Physics **20**(22), 15149 (2018).
[3] M. M. Zalduendo, J. Langer, J. J. Giner-Casares, E. B. Halac, G. J. A. A. Soler-Illia, L. M. Liz-Marzán, P. C. Angelomé, The Journal of Physical Chemistry C **122**(24), 13095 (2018).
[4] H. P. Li, Y. H. Zhu , H. M. Cao, X. L. Yang, C. Z. Li, Materials Research Bulletin **48**(2), 232 (2013).
[5] M. Y. Wang, L. Sun, Z. Q. Lin, J. H. Cai, K. P. Xie, C. Q. Lin, Energy & Environmental Science **6**(4), 1211(2013).
[6] H. T. Li, X. D. He, Z. H. Kang, H. Huang, Y. Liu, J. L. Liu, S. Y. Lian, C. H. Tsang, X. B. Yang, S. T. Lee, Angewandte Chemie International Edition **49**(26), 4430 (2010).
[7] Z. Noreen, N. R. Khalid, R. Abbasi, S. Javed, I. Ahmad, H. Bokhari. Materials Science and Engineering C **98**, 125 (2019).
[8] T. Wang, T. Tang, Y. Gao, Q. Chen, Z. M. Zhang, H. Q. Bian. Physica E: Low-dimensional Systems and Nanostructures **112**, 128(2019).
[9] X. Wang, X. J. Wang, J. F. Zhao, J. K. Song, J. Y. Wang, R. Y. Ma, J. X. Ma, Chemical Engineering Journal **320**, 253 (2017).
[10] I. H. Tseng, W. C. Chang, J. C. S. Wu, Applied Catalysis B: Environmental **37**, 37 (2002).
[11] S. Y. Qin, F. Xin, Y. D. Liu, X. H. Yin, W. J. Ma, Journal of Colloid Interface Science **356**, 257 (2011).
[12] Y. Zhou, Y. W. Wu, Y. H. Li, Y. H. Liu, L. Y. Yang, L. P. Wang, H. Liu, D. D. Li, Q. S. Luo, Ceramics International **42**(10), 12482 (2016).
[13] X. Wang, X. Wang, J. Zhao, J. Song, L. Zhou, J. Wang, X. Tong, Applied Catalysis B: Environmental **206**, 479 (2017).
[14] Y. Zhang, T. Wang, M. Zhou, Y. Wang, Z. Zhang, Ceramics International **43**(3), 3118 (2007).
[15] B. Pant, P. S. Saud, M. Park, S. Park, H. Kim, Journal of Alloys and Compounds **671**, 51 (2016).
[16] X. J. Bai, C. P. Sun, D. Liu, X. H. Luo, D. Li, J. Wang, N. X. Wang, X. J. Chang, R. L. Zong, Y. F. Zhu, Applied Catalysis B: Environmental **204**, 11(2017).
[17] A. Giampiccolo, D. M. Tobaldi, S. G. Leonardi, B. J. Murdoch, M. P. Seabra, M. P. Ansell, G. Neri, R. Ball, Applied Catalysis B: Environmental **243**, 183 (2019).
[18] X. Li, J. G. Yu, M. Jaroniec, X. B. Chen. Chemical Reviews **119**(6), 3962 (2019).
[19] L. Lin, H. Y. Wang, P. Xu, Chemical Engineering Journal **310**, 389(2017).
[20] T. S. Anirudhan, F. Shainy, J. Christa. Journal of Hazardous Material **324**, 117 (2017).
[21] J. X. Guo, Y. Y. Li, S. D. Li, X. M. Cui, Y. Liu, W. Huang, L. N. Mao, X. B. Wei,

X. S. Zhang, Chinese Journal of Catalysis **41**(8), 1208 (2020).
[22] H. Qiu, X. J. Ma, C. Y. Sun, B. Zhao, F. Chen. Applied Surface Science **506**, 145021 (2020).
[23] H. Khan, N. Usen, C. B. Daria, Journal of Enviromental Chemical Engineering **7**(4), 103267 (2019).
[24] X. L. Zheng, D. Q. Zhang, Y. Gao, Y. C. Wu, Q. Y. Liu, X. X. Zhu, Inorganic Chemistry Communications **110**, 107589 (2019).
[25] C. Hong, W. B. Ma, X. Zheng, S. Z. Yan, K. Z. Li, J. L. Guo, J. Lei. Colloids and Surfaces A: Physicochemical and Engineering Aspects **586**, 124283 (2020).
[26] O. R. Isidoro, H. Rafael, M. Alejandro, M. Alejandro, G. Carlos, E. A. Luis, I. S. EnricBrillas, E. Karen, Separation and Purification Technology **224**, 189 (2019).
[27] T. H. Tan, J. Scott, H. N. Yun, R. A. Taylor, K. F. Agueyzinsou, R. Amal, ACS Catalysis **6**(3), 1870 (2017).
[28] M. T. Guo, X. B. Tian, Journal of Hazardous Materials **380**, 120877 (2019).
[29] A. Dhakshinamoorthy, S. Navalon, A. Corma, H. Garcia, Energy Environment Science **5**, 9217(2012).
[30] Y. S. Chen, B. K. Chao, N. G. Tadaaki, C. H. Hsueh. Materials Chemistry and Physics **240**, 122216 (2020).
[31] M. B. Laleh, K. J. Ayoub, N. H. Seyed, P. Mahdi, Process Safety and Environmental Protection **122**, 328 (2019).
[32] Y. L. Kuo, H. W. Chen, Y. Ku, Thin Solid Films **515**, 3461 (2007).
[33] P. O. Shirley, N. D. Paul, M. M. Fanyana, J. K. Michael. O. O. Bamidele, P. Vusumzi, Journal of Environmental Management **260**, 110145 (2020).
[34] L. X. Zhang, C. H. Ni, H. F. Jiu, C. M. Xie, J. B. Yan, G. S. Qi, Ceramics International **43**, 5450 (2017).
[35] E. Tao, Z. Y. Ma, S. Y. Yang, Y. Li, D. Ma, Z. Q. Xing, Y. Li, Journal of Alloys and Compounds **827**, 154280 (2020).
[36] J. J. Fan, S. W. Liu, J. G. Yu, Journal of Materials Chemistry **22**, 17027 (2012).
[37] N. R. Khalid, Z. Hong, E. Ahmed, Y. Zhang, H. Chan, M. Ahmad, Applied Surface Science **258**, 5827 (2012).
[38] W. J. Zhao, Z. C. Zhang, J. Zhang, H. G. Wu, L. M. Xi, C. H. Ruan, Materials Letters **171**, 182 (2016).
[39] E. Z. Liu, L. M. Kang, F. Wu, T. Sun, X. Y. Hu, Y. H. Yang, H. C. Liu, J. Fan, H. C. Liu, J. Fan, Journal of Plasmonics **9**, 61 (2014).
[40] L. M. Martinez, A. Munoz, M. A. Centeno, J. A. Odriozola, Journal of Raman Spectroscopy **47**(2), 189 (2016).
[41] T. L. Guo, J. G. Li, X. D. Sun, Y. S. Sakka. Applied Surface Science **423**, 1 (2017).
[42] Y. Zhou, X. P. Ou Yang, Y. Wang, L. X. Liu, W. J. Zhu, Acta Materiae Compositae Sinica **35**(2), 384 (2018).
[43] Y. F. Wang, M. Zhang, H. Yu, Y. Zuo, J. Gao, G. He, Z. Q. Sun, Applied Catalysis B: Environmental **252**, 174 (2019).
[44] C. Li, T. Wang, Y. Zhu, S. Y. Zhang, C. J. Mao, J. Y. Wu, B. K. Jing, Y. P. Tian, Applied Surface Science **257**, 6568 (2011).
[45] S. P. Zhang, J. Xu, J. Hu, C. Z. Cui, H. L. Liu, ACS Langmuir **33**(20), 5015 (2017).
[46] Z. Jafari, N. Mokhtariana, G. Hosseinzadehb, M. Farhadian, A. Faghihi, F. Shojaie, Journal of Energy Chemistry **25**, 393 (2016).